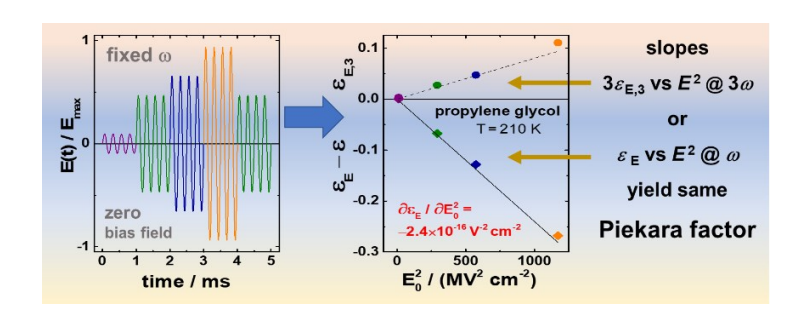
# New experimental approach to nonlinear dielectric effects in the static limit

# Erik Thoms and Ranko Richert

School of Molecular Sciences, Arizona State University, Tempe, Arizona 85287, USA

We present a nonlinear dielectric technique that measures the real and imaginary component of permittivity in a time resolved fashion for a sequence of high field amplitudes. Data is recorded within a few milliseconds of exposing the sample to sinusoidal fields without dc-bias. This short exposure time and a sample thickness of only 10  $\mu$ m greatly reduces heating effects. The Piekara factor quantifying the nonlinear dielectric effect can be derived from analyzing the response at both the fundamental and the third harmonic frequency, and for both quantities the near quadratic field dependence is verified. The small deviations from the expected field dependence are ascribed to a resolved fifth harmonic response. In this manner, the nonlinear dielectric effect of the polar glass-forming liquid propylene glycol is determined in the static limit, and it is found that the Piekara factor changes from  $-2.9 \times 10^{-16} \text{ V}^{-2} \text{ m}^2$  to  $-1.4 \times 10^{-16} \text{ V}^{-2} \text{ m}^2$  when the temperature is raised from 204 K to 235 K.



Keywords: nonlinear dielectric effects, Piekara factor, high electric fields, supercooled liquids

# 1. Introduction

Since Debye recognized that "the dielectric constant would not be a true constant but would depend upon the field intensity" [1], many measurements of this nonlinear dielectric effect (NDE) in the static limit have been reported [2,3,4]. The aim of such experiments is to quantify the difference between the dielectric constant measured at a high electric field,  $\varepsilon_E$ , and its low field limit counterpart,  $\varepsilon_S = \varepsilon_{E\to 0}$ . This difference is usually very small and (to first order) expected to depend quadratically on the amplitude E of the electric field. As a result, it is common to express the magnitude of the NDE in terms of the Piekara factor [5],

$$a = \frac{\varepsilon_E - \varepsilon_{E \to 0}}{E^2},\tag{1}$$

which can assume negative (explained by dielectric saturation) and positive (often termed as chemical effect) values [6].

The motivation for experimentally quantifying NDEs originates from the recognition that high field permittivities are able to reveal information about the material to which the linear-response dielectric experiments are blind [7,8,9,10,11]. This has led to a recent surge in the interest in nonlinear dielectric studies beyond the static limit, as these studies advanced our understanding of interactions, structure, dynamics, and phase transitions in liquids and glasses [12,13,14,15,16,17,18,19,20,21,22,23,24]. A quantitative characterization of NDE's may also help understanding dielectric breakdown [25] and optimize high energy capacitors.

A survey of the literature reveals that considerable discrepancies regarding the Piekara factor can be found. For instance, values for diethyl ether at 25°C vary between  $+1.5\times10^{-18}$  V<sup>-2</sup> m<sup>2</sup> and  $-220\times10^{-18}$  V<sup>-2</sup> m<sup>2</sup> [26]. There are numerous obstacles to a reliable measurement of the Piekara factor, most notably the following examples. (i) Most importantly, the difference  $\varepsilon_E - \varepsilon_{E\to 0}$  is usually small at practical field amplitudes, with the field magnitudes limited by dielectric breakdown of the sample. (ii) Electrostriction leads to a reduction of the electrode separation d, and thus to an apparent change in permittivity via a real change in the geometric capacitance,  $C_{geo} = \varepsilon_0 A/d$ . (iii) Time dependent fields give rise to an irreversible energy transfer from the field to the sample, eventually leading to heating and the concomitant modifications of the dielectric constant and density. In the special case of sinusoidal fields,  $E(t) = E_0 sin(\omega t)$ , heating effects are proportional to  $\varepsilon''(\omega)E^2$ , where  $\varepsilon''$  represents the dielectric loss. But generally, any time dependent field will lead to heating whenever  $\varepsilon'' > 0$ .

Many experiments aimed at quantifying the Piekara factor are based upon a small amplitude oscillating field superposed on a short but high amplitude field pulse. The idea is to restrict the time available for heating via the inevitable dc-conductivity of polar materials. However, for the short time in which a system behaves adiabatically, the reduction of configurational entropy by polarizing the dielectric will be balanced by additional heat [27], leading to a temperature increase as in electrocaloric materials [28]. A further detrimental effect of dc-conductivity is electrode polarization, leading to a rise in the apparent dielectric constant by space charge accumulation at the electrodes, an effect that is promoted by relatively low frequencies or by dc-bias fields.

This work focuses on the permittivity in the static limit, where the polarization follows the electric field without lag. For the experiment, this implies that measurements need to determine permittivity in the long-time limit relative to the primary dielectric relaxation process. Our approach to measuring the Piekara factor eliminates the application of a dc-bias field, but instead uses a sequence of sinusoidal fields of varying field amplitude, with permittivity analyzed for each cycle. The technique facilitates verifying the quadratic field dependence of  $\varepsilon_E$  and the time invariance of  $\varepsilon_E$  after changing the field amplitude. Heating effects are strongly reduced by using an electrode distance of 9.2  $\mu$ m, leading to highly efficient heat transport to the electrodes, which can be regarded as high capacity thermal reservoirs. For propylene glycol (PG) we find that the Piekara factor changes from  $-2.9 \times 10^{-16} \text{ V}^{-2} \text{ m}^2$  to  $-1.4 \times 10^{-16} \text{ V}^{-2} \text{ m}^2$  when the temperature is raised from 204 K to 235 K. Consistency is observed for values derived from the evaluation at the fundamental frequency and those obtained from the third harmonic responses.

## 2. Experiment

The material propylene glycol (PG, >99.5%) has been obtained from Sigma-Aldrich and is used as received. In order to provide a well defined electrode separation, monodisperse silica microspheres with diameter 9.2 µm (Cospheric) are mixed into an aliquot of PG to obtain a composition of approximately 100 ppm by volume. This mixture is filled into a spring-loaded (force: 10 N) capacitor cell described previously [29], using a pair of titanium electrodes with 17 mm and 20 mm diameter. The cell is mounted onto the cold finger of a closed cycle He-refrigerator cryostat (Leybold RDK 6-320, Coolpak 6200), and its temperature is controlled by a Lakeshore Model 340 equipped with DT-470-CU diode sensors. The chamber was flushed with dry nitrogen gas and subsequently evacuated prior to performing the measurements.

The field pattern applied to the sample is derived from an arbitrary waveform generator (Stanford Research Systems DS-345). The voltage of the generator signal is boosted by a factor of 100 via a high-

voltage amplifier (Trek PZD-350), whose output is connected to the high-potential side of the sample capacitor. The low-potential side of the capacitor is connected to ground via an R = 300 or  $1000 \Omega$  shunt. Both electrode potentials,  $V_{hi}$  and  $V_{lo}$ , are measured with a data acquisition system (Nicolet Sigma 100) and yield the voltage across ( $V = V_{hi} - V_{lo}$ ) and the current through ( $I = V_{lo}/R$ ) the capacitor. Figure 1 shows a typical signal pattern, but for clarity with half the number of cycles per zone relative to what is actually used. Within each zone the amplitude is constant, and the entire waveform is repeated 5000 times at a slow repetition rate, such that the duty cycle remains below 10% and the voltage is maintained at zero for at least 90% of the time. The data acquisition system then averages over the 5000 waveforms of V(t) and I(t), recorded at a resolution of 12 bit with 250 points per cycle. All measurements are performed at frequencies sufficiently below the loss peak frequency  $v_{max}$ , such that the real part of the high field permittivity corresponds to the static limit  $\varepsilon_E$ .

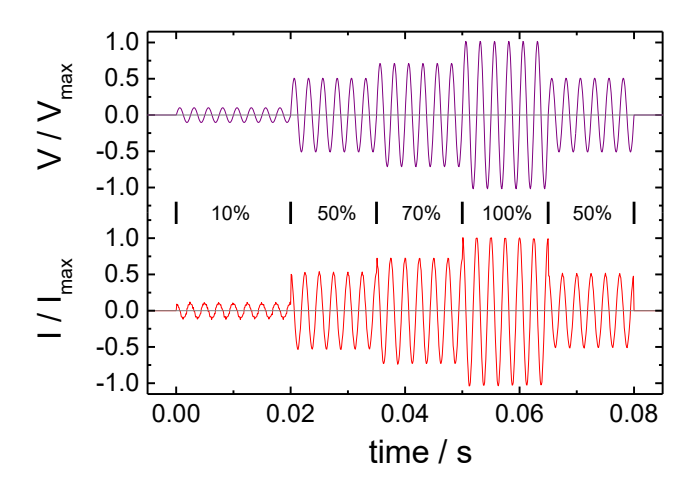


**Fig. 1.** Representation of the field pattern used in this study, with the top curve showing the voltage normalized to its peak value, while the bottom curve reflects the normalized current from a 10 nF capacitor. Each of the five zones (numbered 1 to 5 in the order of increasing time) is associated with its distinct value of  $V_{peak}/V_{max}$ , indicated as percentage value, while frequency and phase remains constant across the entire waveform. The actual experiments with PG employed twice the number of cycles per zone relative to this graph.

In order to obtain time-resolved permittivity data, each period with duration  $2\pi/\omega$  of the voltage and the current signal is subject to Fourier analysis, yielding the in-phase (S') and out-of-phase (S'') component of the  $n^{th}$  harmonic, according to

$$S'_{n} = \frac{\omega}{\pi} \int_{t}^{t+2\pi/\omega} \sin(n\omega t') S(t') dt', \qquad (2a)$$

$$S_{n}^{"} = \frac{\omega}{\pi} \int_{t}^{t+2\pi/\omega} \cos(n\omega t') S(t') dt', \qquad (2b)$$

respectively, where S = V for voltage and S = I for current. For each harmonic (n = 1, 3), amplitudes  $|S_n|$  and phases  $\varphi_{S_n}$  of each of the two signals are determined from the relations  $|S_n| = \left(S_n^{'2} + S_n^{''2}\right)^{1/2}$  and  $\varphi_{S_n} = \arctan(S_n^{''}/S_n^{'})$  [30]. Based on the resulting values for  $|V_1|$ ,  $\varphi_{V_1}$ ,  $|I_1|$ ,  $\varphi_{I_1}$ ,  $|I_3|$ , and  $\varphi_{I_3}$ , 'permittivity' values for the fundamental and third harmonic responses can be obtain for each period using

$$|\varepsilon_n| = \frac{|I_n|/|V_1|}{n\omega C_{aeo}},\tag{3a}$$

$$\varepsilon_n' = |\varepsilon_n| \sin(\varphi_{I_n} - \varphi_{V_1}), \tag{3b}$$

$$\varepsilon_n^{"} = |\varepsilon_n| \cos(\varphi_{I_n} - \varphi_{V_1}). \tag{3c}$$

Note that the voltage has only a fundamental frequency component, i.e.,  $|V_3| = 0$ . As this study focuses on the dielectric constant in the static limit ( $\omega << 1/\tau_\alpha$ ),  $\varepsilon'_1$  will be denoted as  $\varepsilon_E$ , and  $\varepsilon'_3$  as  $\varepsilon_{E,3}$ , with  $\varepsilon'_1$  and  $\varepsilon'_3$  defined via Eq. (3b). Note that Eq. (3a) defines  $\varepsilon_n$  by normalizing to  $|V_1|$  instead of  $|V_1|^n$ . As a result,  $\varepsilon_{E,3}$  has no units and depends on the field magnitude. For each period, the average power,  $p_{avg}$ , transferred to the sample is also calculated according to

$$p_{avg} = \frac{\omega}{2\pi} \int_{t}^{t+2\pi/\omega} V(t') I(t') dt', \qquad (4)$$

so that the resulting temperature increase of the sample can be estimated.

The permittivity of PG in the low field (linear response) limit has been measured with a Solartron SI-1260 gain/phase analyzer equipped with a DM-1360 transimpedance amplifier. To this end, the same cell used for the high-field experiments has been employed, but with a 100 µm thick Teflon ring as spacer instead of the microspheres, see inset of Fig. 2.

## 3. Results

For the low field ( $E_0 = 0.1 \text{ kV cm}^{-1}$ ) experiment, both the real ( $\varepsilon'$ ) and imaginary components ( $\varepsilon''$ ) versus frequency are depicted in Fig. 2 for temperatures covering the range in which high-field data is taken. The dielectric relaxation behavior observed here is consistent with previous reports [31,32]. From a comparison of the observed static dielectric constant values,  $\varepsilon_s$ , with those reported by Davidson and Cole, we determine the actual electrode separation. For the low field experiment, we found  $d = 106 \mu \text{m}$ 

for the Teflon spacer with 100  $\mu$ m nominal thickness. For the high-field cases, the actual electrode distance was  $d = 10.5 \mu$ m, slightly higher than the nominal silica microsphere diameter of 9.2  $\mu$ m. It has been demonstrated earlier by Bauer *et al.* [33] that such microspheres do not affect high field dielectric measurements adversely and do not lead to Maxwell-Wagner polarization.

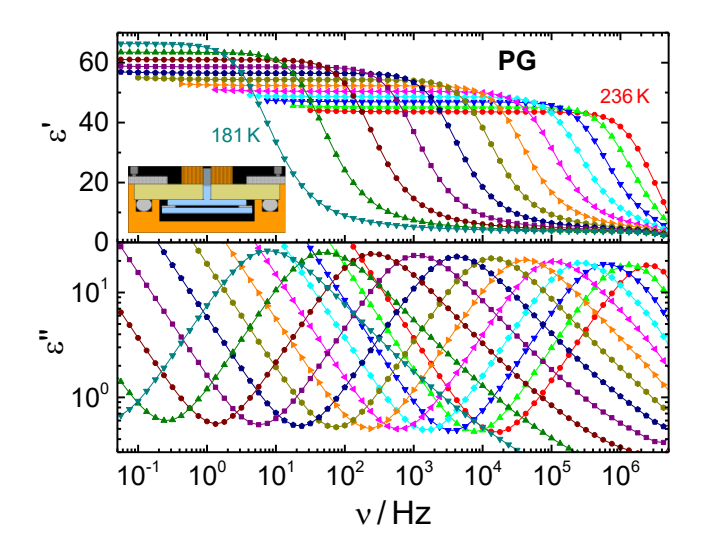


**Fig. 2.** Plot of  $\varepsilon'$  and  $\varepsilon''$  versus frequency for PG at temperatures from T = 181 to 236 K in steps of 5 K. The  $\varepsilon''$  spectra are used to locate the frequency of minimum loss,  $v_{min}$ , between dc-conductivity and relaxation peak for each temperature, with  $v_{min}$  representing an ideal frequency for the high-field experiment. The inset shows a schematic cut view of the dielectric cell, the details of which can be found in Ref. [29].

As true for most measurements of permittivity, we derive  $\varepsilon$  from the impedance of a planar capacitor filled with the sample. We also follow common practice and evaluate the high field analogue,  $\varepsilon_E$ , in the same manner as in the regime of linear response, see Eq. (3). An example of an experiment using the field pattern of Fig. 1 is depicted in Fig. 3, which shows both the real and imaginary components of the high field permittivity,  $\varepsilon'_I$  and  $\varepsilon''_I$ , respectively. It is obvious that  $\varepsilon'_I$  is practically time invariant within each zone (region of constant field amplitude  $E_0$ ), whereas  $\varepsilon''_I$  changes considerably even while  $E_0$  is constant. Because this effect is reduced at higher frequencies (not shown), free charges leading to deconductivity are the most likely cause. Consequently, the following focuses on  $\varepsilon_E = \varepsilon'_I$ .

The field induced relative change of  $\varepsilon_E$  is shown as  $(\varepsilon_E - \varepsilon)/\varepsilon$  versus time for three different temperatures in Fig. 4, where the field reaches up to 340 kV cm<sup>-1</sup>. For each temperature the frequency is selected to lead to a small value of the dielectric loss, near the minimum between the contributions from

dc-conductivity and primary relaxation process, see Fig. 2. Such measurements have been performed at seven different temperatures between 204 and 235 K, but for clarity only a selection is shown in Fig. 4. The measurements leading to the data in Fig. 4 have also been analyzed at 3 $\omega$ , and the real part of the third harmonic permittivity,  $\varepsilon_{E,3}$ , is shown in Fig. 5.

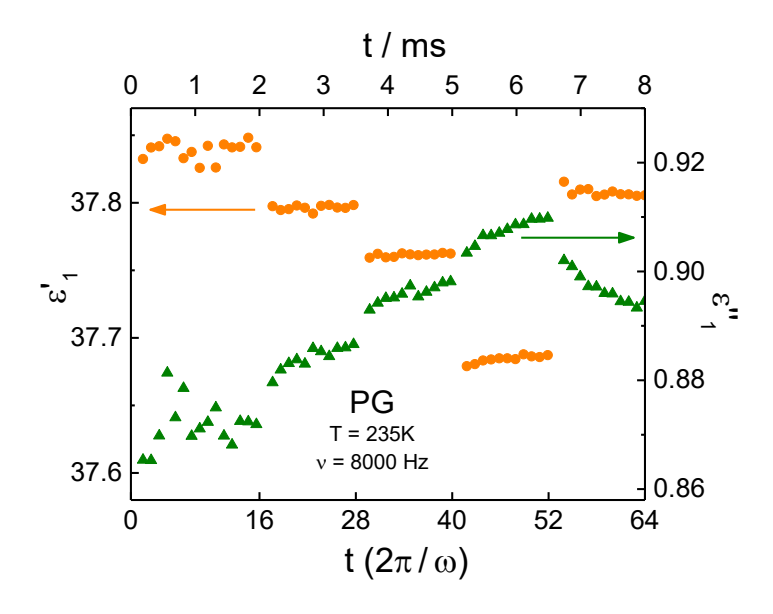


**Fig. 3.** Results for the high field permittivity,  $\varepsilon'_1$  and  $\varepsilon''_1$ , of PG at T = 235 K, derived from the signals  $V_1(t)$  and  $I_1(t)$ , i.e., at the fundamental frequency v = 8 kHz. The highest peak field (100%, zone 4, periods 40 to 52, see lower axis) is  $E_0 = 340$  kV cm<sup>-1</sup>.

Data such as those shown in Fig. 4 and Fig. 5 are further analyzed by calculating the average value of  $\varepsilon_E$  or  $\varepsilon_{E,3}$  within each zone of constant  $E_0$ . For each temperature, this generates two sets of field dependent permittivities,  $\varepsilon_E(E_0)$  and  $\varepsilon_{E,3}(E_0)$ . For the T=210 K case, this field dependence is depicted versus the square of the field amplitude in Fig. 6, with the straight lines indicating consistency with the expected quadratic dependence on the electric field  $E_0$ .

In a final experiment, we deviate from the field pattern of Fig. 1. Instead of further increasing the field in zone 4, the frequency is increased by a factor of 4. As expected, the quantity  $(\varepsilon_E - \varepsilon)/\varepsilon$  at  $\nu = 4$  kHz changes a factor of four when the field is increased by a factor of two, and it reverts to the same lower value when the field is reduced again. The main feature of this experiment is that  $\varepsilon_E$  is practically not affected by an increase in frequency by a factor of four, or by the concomitant increase in power by a factor of about 5.

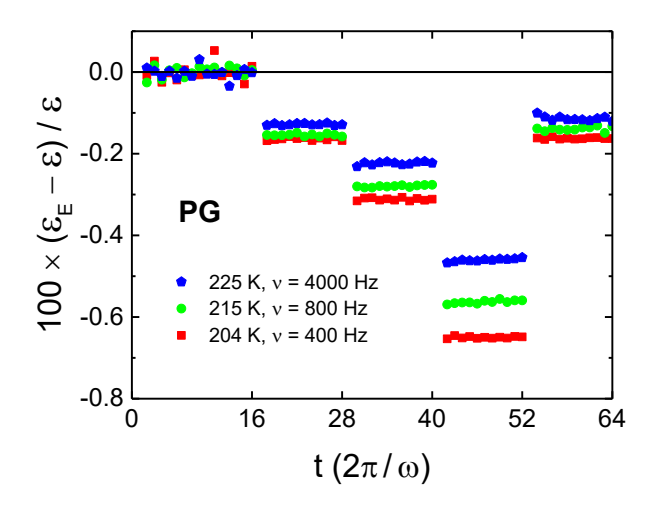


**Fig. 4.** Results for the field induced relative change of the dielectric constant,  $(\varepsilon_E - \varepsilon)/\varepsilon$  ( $\approx \ln \varepsilon_E - \ln \varepsilon$ ), for PG at temperatures T = 225, 215, and 204 K, using the respective frequencies 4000, 800, and 400 Hz. For each case, the highest peak field (100%, zone 4) is  $E_0 = 340 \text{ kV cm}^{-1}$ .

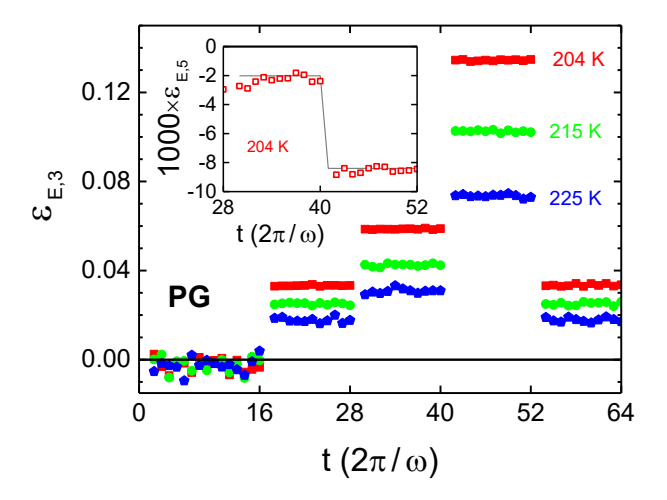


**Fig. 5.** Results for the third harmonic dielectric constant,  $\varepsilon_{E,3}$ , for PG. From top to bottom curve, the temperatures are T = 204, 215, and 225 K, and the frequencies used are 400, 800, and 4000 Hz (same colors and symbols as in Fig. 4). For each case, the highest peak field (100%, zone 4) is  $E_0 = 340 \text{ kV}$  cm<sup>-1</sup>. The inset shows the fifth harmonic analogue,  $\varepsilon_{E,5}$ , for T = 204 K, with the line indicating a change from  $2.02 \times 10^{-3}$  to  $8.4 \times 10^{-3}$  as the field is increased from 238 to 340 kV cm<sup>-1</sup>.

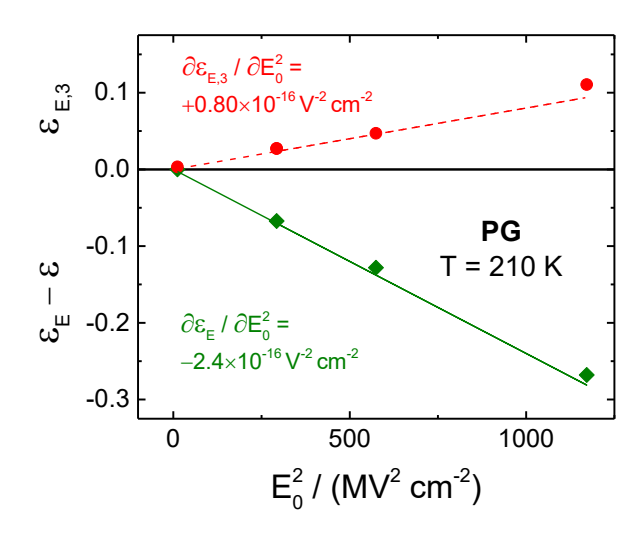


**Fig. 6.** Representative field dependence of  $\varepsilon_E - \varepsilon$  (green diamonds) and of  $\varepsilon_{E,3}$  (red circles) for PG at T = 210 K, derived from measurements as depicted in Fig. 4 and Fig. 5, respectively. The solid line is a fit to  $\varepsilon_E = aE_0^2$  with slope  $a = -2.4 \times 10^{-16}$  V<sup>-2</sup> cm<sup>2</sup>, the dashed line represents  $\varepsilon_{E,3} = -aE_0^2/3$  with the same value for a.

#### 4. Discussion

A typical approach to determining the Piekara factor is to measure permittivity via a small amplitude oscillating field of appropriate frequency during the application of a high field pulse with amplitude  $E_B$  [34,35]. The values of  $\varepsilon$  and  $\varepsilon$  are obtained from the capacitances  $C = \varepsilon C_{geo}$  at zero and high bias field  $E_B$ , with C derived from the resonance frequency of an LC circuit. As has been demonstrated recently [36], the typical manner to obtain  $\varepsilon$  does not yield a material specific quantity. Instead, the values for  $\varepsilon$  derived from a field  $E(t) = E_B + E_0 sin(\omega t)$  will differ for the two limiting cases,  $E_B >> 0$  and  $E_0 \to 0$  versus  $E_B = 0$  and  $E_0 >> 0$ . An appropriate quantity to specify the nonlinear dielectric behavior of a material in the static limit is  $\chi_3$ , defined as higher order susceptibility via

$$\varepsilon_0^{-1} P = \chi E + \chi_3 E^3 \,, \tag{5}$$

where  $\varepsilon_0$  is the permittivity of vacuum. For a given value of this third order susceptibility and disregarding higher order terms, it can be shown that the relations between  $\chi_3$  and the present experimental results  $\varepsilon_E$  and  $\varepsilon_{E,3}$  are given by [36]

$$\frac{(\varepsilon_E - \varepsilon)}{E_0^2} = \frac{\partial \varepsilon_E}{\partial E_0^2} = \frac{3}{4} \chi_3 \,, \tag{6}$$

$$\frac{\varepsilon_{E,3}}{E_0^2} = \frac{\partial \varepsilon_{E,3}}{\partial E_0^2} = -\frac{1}{4} \chi_3 , \qquad (7)$$

respectively. For the common high static field case,  $E_B >> 0$  and  $E_0 \to 0$ , the relation reads

$$\frac{(\varepsilon_E - \varepsilon)}{E_R^2} = a = 3\chi_3 \,, \tag{8}$$

cf., Eq. (1). For a quantitative comparison of results from different approaches, it thus seems advantageous to resort to the technique invariant and material specific quantity  $\chi_3$ . It is important to realize that the notation  $|\chi_3|$  is commonly used for experimental results of frequency dependent NDEs derived from third harmonic responses, and is thus more equivalent to the present  $|\varepsilon_{E,3}|E_0^2$  and not the same as  $\chi_3$  used in this work and defined in Eq. (5).

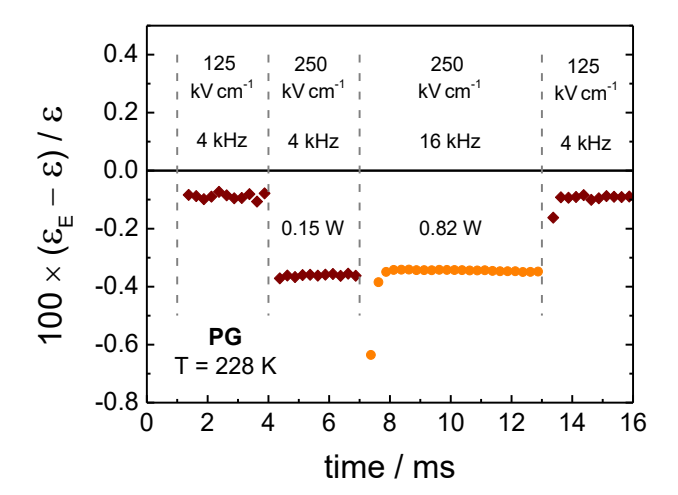
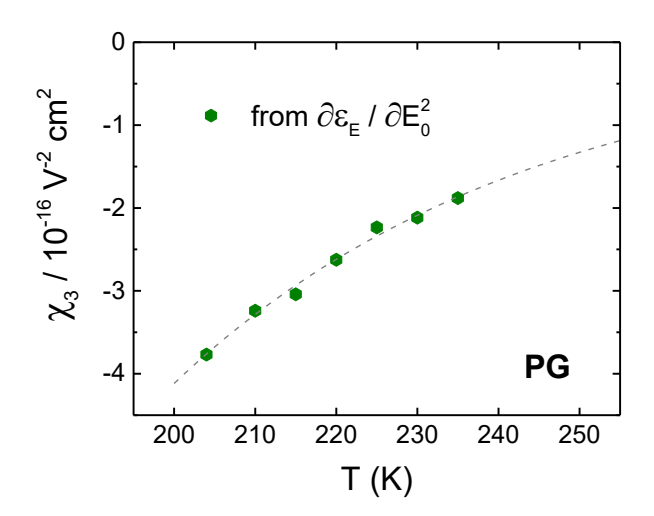


Fig. 7. Results for the field induced relative change of the dielectric constant,  $(\varepsilon_E - \varepsilon)/\varepsilon$  ( $\approx \ln \varepsilon_E - \ln \varepsilon$ ), for PG at a temperature T = 228 K, using two frequencies. The electric fields and frequencies applied in each zone are provided in the legend. For the two high-field zones, the average power transferred irreversibly to the sample is also listed, 0.15 and 0.82 W, as determined via Eq. (4). For the first four periods only 25 kV cm<sup>-1</sup> are applied (not shown), so that the sample can equilibrate with the oscillating field.

Based upon Eq. (6) and Eq. (7), the slopes  $\partial \varepsilon_E/\partial E_0^2$  and  $\partial \varepsilon_{E,3}/\partial E_0^2$  are expected to differ by a factor of -3. Figure 6 validates this by demonstrating that both quantities depend quadratically on the electric field and by showing that the slope  $-\partial \varepsilon_E/3\partial E_0^2$  (dashed line) agrees within 15% with the slope  $\partial \varepsilon_{E,3}/\partial E_0^2$  at T=210 K. At all temperatures, the deviations between the  $\chi_3$  results from the first and third harmonic data remain less than 20%. Some deviation is expected on the basis of having disregarded higher order susceptibilities such as  $\chi_5$  in Eq. (5). The feature that higher orders cannot be omitted entirely

can be observed in the inset of Fig. 5, clearly showing a fifth order contribution with the expected field dependence,  $\varepsilon_{E,5} \propto E_0^4$ . Its contribution is about 10% of that of  $\varepsilon_{E,3}$ , so that  $\varepsilon_{E,5}$  could be a major factor in the small deviation from  $\partial \varepsilon_E / \partial E_0^2 = -3 \partial \varepsilon_{E,3} / \partial E_0^2$  seen in Fig. 6.

Our preference for measuring with a series of three distinct high fields originates from the observation that the low field limit data (see zone 1 in Fig. 4) is associated with small signal amplitudes and thus higher scatter. Using three high-field data points to define  $\partial \varepsilon_E/\partial E_0^2$  eliminates the need to determine the low field limit accurately. Moreover,  $\varepsilon_E(E_0)$  results such as those of the T=210 K case shown in Fig. 6 also facilitate the verification of the expected quadratic field dependence to ensure consistency. The slopes  $\partial \varepsilon_E/\partial E_0^2$  have been evaluated for all temperatures and converted to  $\chi_3$  values. The  $\chi_3(T)$  values obtained in this manner for PG are compiled in Fig. 8. In the T=204 to 235 K range, a reduction of the nonlinearity in terms of  $\chi_3$  by a factor of 2 is observed. An extrapolation along the exponential dashed line would suggest that the NDE becomes negligible at a temperature around 370 K.



**Fig. 8.** Third harmonic susceptibility  $\chi_3$  for PG versus temperature, derived from  $\partial(\varepsilon_E - \varepsilon)/\partial E_0^2$  (solid hexagons). The dashed line represents the relation  $\chi_3 = A \times \exp(-T/B)$  with  $A = -3.8 \times 10^{-14}$  V<sup>-2</sup> cm<sup>2</sup> and B = 44.2 K, and is meant to serve as guide.

We now turn to the effects that may lead to apparent nonlinear behavior: field-induced heating and electrostriction. To approximate the heating effects, we consider the highest power that occurred in the course of the present experiments leading to the results of Fig. 8, which was P = 0.67 W, reached for the situation given by T = 235 K, v = 8 kHz, and  $E_0 = 340$  kV cm<sup>-1</sup>. We assume that the metal electrodes positioned at z = 0 and z = d are heat sinks of infinite heat capacity, so that the temperature increase  $\Delta T$  vanishes at the interfaces. The steady state heat equation for this situations reads  $\partial^2 \Delta T(z)/\partial z^2 = -p/\kappa$ ,

where p is the power density (p = power P divided by volume v) and  $\kappa$  the thermal conductivity. The solution to the average temperature rise is

$$\Delta T_{avg} = \frac{Pd^2}{12\kappa v}. (9)$$

With P = 0.67 W, d = 10.5 µm,  $v = 2.4 \times 10^{-9}$  m<sup>3</sup>, and  $\kappa = 0.2$  W m<sup>-1</sup> K<sup>-1</sup> [37], the average increase in temperature is  $\Delta T_{avg} = 19$  mK, and the peak value at z = d/2 is only 50% higher. Using the data of Davidson and Cole [31] for PG to evaluate the temperature sensitivity of  $\varepsilon$ , we obtain  $\partial \varepsilon / \partial T = -0.26$  K<sup>-1</sup> at T = 235 K. Therefore, the effect of heating on  $\varepsilon$  amounts to  $\partial \varepsilon / \partial T \times \Delta T_{avg} = -5 \times 10^{-3}$ , which is only a small fraction (3%) of the change  $\varepsilon_E - \varepsilon = -0.16$  observed at these conditions.

The time required to establish a temperature difference  $\Delta T_{avg}$  can be estimated by equating the thermal diffusivity  $\alpha = \kappa/(\rho C_p)$  with the mean square displacement ( $\lambda$ ) per unit time, i.e.,  $\alpha = \lambda^2/\tau_T$ . Here,  $\rho$  is the mass density and  $C_p$  is the specific heat capacity. Setting  $\lambda = d/2$ , this yields

$$\tau_T = \frac{d^2 \rho c_p}{4\kappa} \,. \tag{10}$$

With  $C_p = 2.0$  J K<sup>-1</sup> g<sup>-1</sup> [38] and  $\rho = 1.08$  g cm<sup>-3</sup>, we estimate  $\tau_T = 0.3$  ms, equivalent to 5 periods at the highest frequency used. Therefore, if heating were a significant contribution to the nonlinear effect, this time dependence should be discernable in data such as those shown in Fig. 4.

Even more convincing regarding the lack of a significant heating effect is the experimental result shown in Fig. 7. By changing only the frequency from 4 to 16 kHz, the power absorbed from the field is increased about fivefold, from 0.15 to 0.82 W. At the temperature of this experiment, T = 228 K, both frequencies, 4 and 16 kHz, are positioned within the plateau region of  $\varepsilon'(\omega)$ . The observation that the data for  $\varepsilon_E$  reveals only a minor sensitivity to this frequency and power change thus implies the absence of a significant heating effect.

The second commonly encountered effect giving rise to apparent NDE, electrostriction, originates from the attractive force of the oppositely charged sample surfaces/electrodes. This force produces stress on the electrodes and tends to lower their distance, thus increasing geometric capacitance and creating an apparent change in permittivity. For a sinusoidal field with  $E(t) = E_0 sin(\omega t)$ , the resulting force has a steady state component  $F_0$  and a second harmonic component given by  $F_0 cos(\omega t)$ . The value of  $F_0$  is determined by

$$F_0 = \frac{\varepsilon \varepsilon_0 A E_0^2}{4} \,. \tag{10}$$

For the present case with  $\varepsilon = 48$  ( $T \approx 220$  K),  $A = \pi (8.5 \text{ mm})^2$ , and  $E_0 = 340$  kV cm<sup>-1</sup> in the 100% field zone, this electrostatic force is 27 N. The microsphere concentration should supply a uniform support of 43 silica beads (on average) across the area A. For the lower fields of the zones, the force  $F_0$  is only a fraction of that of the spring pushing the electrodes together (10 N). Moreover, the spring-loaded electrodes together with the absence of elasticity at the condition  $\omega \tau \ll 1$  argue against the electrode separation periodically adjusting to the sinusoidal change of  $E_0$ . Therefore, a significant impact resulting from electrostriction appears unlikely.

Finally, we compare the present technique with the common high-field pulse method, where permittivity is derived from the resonance frequency of an LC oscillator [34,35]. The pulse technique implies that the NDE is derived from  $\varepsilon_E$  at a high dc-field and the low field limit,  $\varepsilon$ , so that multiple experiments are required to validate the quadratic field dependence. Electrode separations are typically around 500  $\mu$ m for these setups, thus 50 times larger than in the present case, which corresponds to a heat diffusion that is  $50^2$  times less effective than with  $d = 10 \mu$ m. Therefore, large electrode separations may require levels of dc-conductivity and  $\varepsilon''$  below what can be achieved with many polar materials to avoid significant heating.

In comparison to previous approaches, the present technique derives the NDE from the slope of  $\varepsilon_E$  versus  $E^2$  defined via several high field data points, so that possible deviations from the quadratic field dependence can be detected. The manner in which V(t) and I(t) traces are analyzed facilitate focusing on the real part of permittivity, which is not directly influenced by dc-conductivity. Moreover, the data allows us to assess the time dependence of  $\varepsilon_E$  and the power transferred irreversibly from field to sample, which helps identifying potential heating effects.

# 5. Summary and Conclusions

This study has demonstrated several advantages of the present technique aimed at measuring nonlinear dielectric effects in the case of the static limit, i.e., for situations in which the polarization remains in equilibrium with the electric field. The main idea is to apply an alternating field (without dcbias) which is subject to a sequence of field amplitudes. The amplitude remains constant for several periods within each amplitude zone, see Fig. 1, and permittivity is evaluated for each period. High resolution is obtained by averaging over thousands of such field sequences, using a low repetition rate.

A set of voltage and current traces obtained in this manner provide several data points for the field dependence of permittivity,  $\varepsilon_E(E)$ , and its higher harmonics  $\varepsilon_{E,3}(E)$  and  $\varepsilon_{E,5}(E)$ , as well as its time dependence,  $\varepsilon_E(t)$ , after changing the field amplitude. Focusing on the real component of permittivity,  $\varepsilon_E$ , at suitable frequencies reduces the influence of the effects of conductivity, which impacts  $\varepsilon''_I$  more than  $\varepsilon'_I$ . The high field  $\varepsilon_E(E)$  results allows one to verify the expected quadratic field dependence or identify deviations thereof. This approach does not rely on an experimental value for the low field limit,  $\varepsilon$ , which often involves high uncertainties. However, a more reliable  $\varepsilon$  value can be obtained from  $\varepsilon_E(E)$  data by extrapolation to zero field. Observations of time and power invariant  $\varepsilon_E$  results can be used to confirm the absence of heating effects by direct experimental evidence. Although high amplitude alternating fields lead to considerable powers being transferred irreversibly from the field to the sample, the sample thickness of only 10  $\mu$ m guarantees efficient heat diffusion to the electrodes, which act as heat sinks. Using dispersed silica microspheres as spacers appears to counteract electrostriction effectively.

A comparison with the common dc-pulse technique appears in order. The pulse fields with short duration may result in limited heat production, but the relatively large sample dimensions, while suppressing electrode polarization effects, reduce the efficiency of heat diffusion towards the electrode surfaces. Moreover, the present technique allows one to disregard the dielectric loss and thus suppress the influence of a field-dependent conductivity. Both heating and conductivity effects (including electrode polarization) may affect the result and lead to apparently time dependent Piekara factors. We are not aware of literature data on the Piekara factor of PG obtained via the dc-pulse technique for a direct comparison. Thus, future experiments based on the present technique should measure NDE standards such as diethyl ether and nitrobenzene.

The present technique has revealed the following about the high field behavior of PG. In the entire temperature range of this study, dielectric saturation prevails, leading to a field-induced reduction of the dielectric constant. Dielectric saturation should occur in every polar liquid, but its magnitude can not be predicted by current theories. The observed Piekara factor changes from  $-2.9 \times 10^{-16} \, \text{V}^{-2} \, \text{m}^2$  to  $-1.4 \times 10^{-16} \, \text{V}^{-2} \, \text{m}^2$  when the temperature is increased from 204 K to 235 K, with no indication of a transition to the so-called chemical effect, where the sign of the Piekara factor is positive.

## **Declaration of Competing Interest**

The authors declare that they have no known competing financial interests or personal relationships that could have appeared to influence the work reported in this paper.

# Acknowledgments

This research was supported by the National Science Foundation under grant number DMR-1904601.

## References

- [1] P. Debye, Polar Molecules, Chemical Catalog Company, New York, 1929.
- [2] A. Chełkowski, Dielectric Physics, Elsevier, Amsterdam, 1980.
- [3] S. J. Rzoska, V. P. Zhelezny (Eds.), Nonlinear Dielectric Phenomena in Complex Liquids, Kluwer Academic Publishers, Dordrecht, 2004.
- [4] A. Piekara, A. Chelkowski, New experiments on dielectric saturation in polar liquids, J. Chem. Phys. 25 (1956) 794.
- [5] A. Piekara, Dielectric saturation and hydrogen bonding, J. Chem. Phys. 36 (1962) 2145.
- [6] J. Małecki, The relaxation of the nonlinear dielectric effect, J. Mol. Struct. 436-437 (1997) 595.
- [7] D. V. Matyushov, Nonlinear dielectric response of polar liquids, J. Chem. Phys. 142 (2015) 244502.
- [8] S. Albert, Th. Bauer, M. Michl, G. Biroli, J.-P. Bouchaud, A. Loidl, P. Lunkenheimer, R. Tourbot, C. Wiertel-Gasquet, F. Ladieu, Fifth-order susceptibility unveils growth of thermodynamic amorphous order in glass-formers, Science 352 (2016) 1308.
- [9] R. Richert (Ed.), Nonlinear Dielectric Spectroscopy, Springer, Cham, 2018.
- [10] R. Richert, Perspective: Nonlinear approaches to structure and dynamics of soft materials, J. Chem. Phys. 149 (2018) 240901.
- [11] R. Richert, Nonlinear dielectric effects in liquids: A guided tour, J. Phys.: Condens. Matter 29 (2017) 363001.
- [12] J. L. Déjardin, Y. P. Kalmykov, Nonlinear dielectric relaxation of polar molecules in a strong ac electric field: Steady state response, Phys. Rev. E 61 (2000) 1211.
- [13] L. Berthier, G. Biroli, J.-P. Bouchaud, L. Cipelletti, D. El Masri, D. L'Hôte, F. Ladieu, M. Pierno, Direct experimental evidence of a growing length scale accompanying the glass transition, Science 310 (2005) 1797.
- [14] R. L. Fulton, The nonlinear dielectric behavior of water: Comparisons of various approaches to the nonlinear dielectric increment, J. Chem. Phys. 130 (2009) 204503.
- [15] I. Szalai, S. Nagy, S. Dietrich, Nonlinear dielectric effect of dipolar fluids, J. Chem. Phys. 131 (2009) 154905.
- [16] D. L'Hôte, R. Tourbot, F. Ladieu, P. Gadige, Control parameter for the glass transition of glycerol evidenced by the static-field-induced nonlinear response, Phys. Rev. B 90 (2014) 104202.

- [17] S. Samanta, R. Richert, Dynamics of glass-forming liquids. XVIII. Does entropy control structural relaxation times?, J. Chem. Phys. 142 (2015) 044504.
- [18] R. Richert, S. Weinstein, Nonlinear dielectric response and thermodynamic heterogeneity in liquids, Phys. Rev. Lett. 97 (2006) 095703.
- [19] W. Huang, R. Richert, Dynamics of glass-forming liquids. XIII. Microwave heating in slow motion, J. Chem. Phys. 130 (2009) 194509.
- [20] C. Crauste-Thibierge, C. Brun, F. Ladieu, D. L'Hôte, G. Biroli, J.-P. Bouchaud, Evidence of growing spatial correlations at the glass transition from nonlinear response experiments, Phys. ev. Lett. 104 (2010) 165703.
- [21] C. Brun, F. Ladieu, D. L'Hôte, M. Tarzia, G. Biroli, J.-P. Bouchaud, Nonlinear dielectric susceptibilities: Accurate determination of the growing correlation volume in a supercooled liquid, Phys. Rev. B 84 (2011) 104204.
- [22] Th. Bauer, P. Lunkenheimer, A. Loidl, Cooperativity and the freezing of molecular motion at the glass transition, Phys. Rev. Lett. 111 (2013) 225702.
- [23] P. Kim, A. R. Young-Gonzales, R. Richert, Dynamics of glass-forming liquids. XX. Third harmonic experiments of non-linear dielectric effects versus a phenomenological model, J. Chem. Phys. 145 (2016) 064510.
- [24] A. R. Young-Gonzales, S. Samanta, R. Richert, Dynamics of glass-forming liquids. XIX. Rise and decay of field induced anisotropy in the non-linear regime, J. Chem. Phys. 143 (2015) 104504.
- [25] E. Logakis, L. Herrmann, T. Christen, Electric characterization of LDPE films with TSC and dielectric spectroscopy, IEEE Trans. Dielectr. Electr. Insul. 23 (2016) 142.
- [26] Y. Marcus, G. Hefter, On the pressure and electric field dependencies of the relative permittivity of liquids, J. Solution Chem. 28 (1999) 575.
- [27] J. A. Schellman, Dielectric saturation, J. Chem. Phys. 24 (1956) 912.
- [28] J. F. Scott, Electrocaloric materials, Annu. Rev. Mater. Res. 41 (2011) 229.
- [29] K. Adrjanowicz, M. Paluch, R. Richert, Formation of new polymorphs and control of crystallization in molecular glass-formers by electric field, Phys. Chem. Chem. Phys. 20 (2018) 925.
- [30] The actual  $\arctan(x''/x')$  calculation used is:  $\arctan(x''/x')$  for x' > 0,  $[2-sgn(x'')] \times \pi/2$  for x' = 0, and  $\arctan(x''/x') + \pi$  for x' < 0.
- [31] D. W. Davidson, R. H. Cole, Dielectric relaxation in glycerol, propylene glycol, and n-propanol, J. Chem. Phys. 19 (1951) 1484.
- [32] S. Weinstein, R. Richert, Nonlinear features in the dielectric behavior of propylene glycol, Phys. Rev. B 75 (2007) 064302.
- [33] Th. Bauer, M. Michl, P. Lunkenheimer, A. Loidl, Nonlinear dielectric response of Debye, α, and β relaxation in 1-propanol, J. Non-Cryst. Solids 407 (2015) 66.
- [34] M. Gorny, J. Ziolo, S. J. Rzoska, A new application of the nonlinear dielectric method for studying relaxation processes in liquids, Rev. Sci. Instrum. 67 (1996) 4290.

- [35] K. Orzechowski, A. Burakowski, Experimental set-up for measuring the non-linear dielectric effect, Measurement 131 (2019) 219.
- [36] R. Richert, D. V. Matyushov, Quantifying dielectric permittivities in the nonlinear regime, J. Phys. Condens. Matter 33 (2021) 385101.
- [37] C. Deng, K. Zhang, Thermal conductivity of 1,2-ethanediol and 1,2-propanediol binary aqueous solutions at temperature from 253 K to 373 K, Int. J. Thermophys. 42 (2021) 81.
- [38] G. S. Parks, H. M. Huffman, Studies on glass. I. The transition between the glassy and liquid states in the case of some simple organic compounds, J. Phys. Chem. 31 (1927) 1842.